A SEARCH FOR LIGHTLY IONIZING PARTICLES IN THE LUX DETECTOR AND R&D FOR FUTURE EXPERIMENTS

by

KATAYUN J KAMDIN

A dissertation submitted in partial satisfaction of the requirements for the degree of

Doctor of Philosophy

in

Physics

in the

Graduate Division

of the

University of California, Berkeley

Committee in charge:

Professor Daniel McKinsey, Chair
Professor Marjorie Shapiro
Doctor Peter Sorensen
Professor Kai Vetter

Summer 2018

ABSTRACT

A Search for Lightly Ionizing Particles in the LUX Detector and R&D For Future Experiments

by

Katayun J Kamdin

Doctor of Philosophy
University of California, Berkeley
Professor Daniel McKinsey, Chair

Write the abstract here.

To my mom, for always making me feel like I could do this. To my friends, for being there when I was sure I couldn't.

ACKNOWLEDGMENTS

Some Text

More Text.

More text

CONTENTS

LIST OF FIGURES

LIST OF TABLES

ACRONYMS

SM Standard Model

BSM Beyond the Standard Model

SUSY Supersymmetry

MSSM Minimal Supersymmetric Model

cMSSM Constrained MSSM

pMSSM Phenomenological MSSM

LSP Lightest Supersymmetric Particle

WIMP Weakly Interacting Massive Particle

LIP Lightly Ionizing Particle

LUX Large Underground Xenon [Experiment]

LXe Liquid Xenon

SURF Sanford Underground Research Facility

HV High Voltage

SHV Safe High Voltage (a manufacturing identification)

RMS root mean square

1 INTRODUCTION

I was dreamin' when I wrote this, forgive me if it goes astray.

— Prince

This Thesis goes like....

PART I

THEORETICAL CONTEXT AND EXPERIMENTAL STRATEGIES

This section describes the theoretical foundation for the analysis presented in Part II. It includes an overview of the Standard Cosmology...

2

INTRODUCTION

I was dreamin' when I wrote this, forgive me if it goes astray.

— Prince

2.1 A LITTLE HISTORY

Our understanding of the universe develops in a leap-frog of theory and observation, one catching up to and surpassing the other as technology improves, to be passed in turn by a new idea or new observation.

2.2 THE STANDARD COSMOLOGY

The standard cosmology is a parametrization of the Big-Bang cosmological model is also referred to as ΛCDM ("Lambda-CDM") and it accounts for the observed:

- cosmic microwave background (CMB)
- large scale structure of galaxies and clusters
- accelerating expansion of the universe
- abundances of hydrogen and helium

Since the CMB was discovered in 1965

2.3 EVIDENCE FOR DARK MATTER

2.3.1 GALAXIES AND CLUSTERS

2.3.2 COSMIC MICROWAVE BACKGROUND

2.4 DARK MATTER CANDIDATES MOTIVATED BY PARTICLE PHYSICS

2.4.1 WIMPS AND THE HIERARCHY PROBLEM

2.4.2 AXIONS AND THE STRONG CP PROBLEM

2.5 MOTIVATION FOR LIPS

3 PARTICLE DETECTION WITH LIQUID XENON

3.1 LIQUID XENON AS A DETECTOR MEDIUM

3.1.1 RADIOPURITY

3.1.2 SELF-SHIELDING

3.1.3 SCINTILLATION AND IONIZATION

3.1.4 WIMP RATES AND CROSS SECTION

3.2 ER, NR DISCRIMINATION

3.3 DUAL-PHASE LIQUID XENON TIME PROJECTION CHAMBER

3.4 LUX

3.4.1 OPTIMIZATION FOR WIMPS

3.4.2 LIP SEARCH ABILITY

PART II

BIG SCIENCE

This section describes research done with the LUX Detector.

4

THE LUX DETECTOR

4.1 DETECTOR COMPONENTS

4.1.1 CRYOSTAT

4.1.2 PMTS

4.1.3 WATER TANK

4.1.4 TRIGGER AND DATA ACQUISITION

4.2 CALIBRATIONS

4.2.1 TRITIUM

4.2.2 DD

4.2.3 KR

5

LIGHTLY IONIZING PARTICLE SEARCH

5.1 MODELING LIP INTERACTION

5.1.1 FVP CROSS SECTION

5.1.2 STRAGGLING

5.1.3 ENERGY RESOLUTION IN LUX

5.1.4 POSITION RESOLUTION IN LUX

5.2 LIP SEARCH

5.2.1 LUX RUN03 CONDITIONS

5.2.2 LUX RUN04 CONDITIONS

5.3 LIP SEARCH ANALYSIS

5.3.1 ENERGY CONSISTENCY

5.3.2 TRACK LINEARITY CRITERIA

5.3.3 BACKGROUND REJECTION

5.3.4 MUONS

5.3.5 GAMMAS

5.3.6 ELECTRON TRAINS?

5.4 RESULT: VERTICAL FLUX LIMIT

PART III

LITTLE SCIENCE

This section describes research with a small test bed at Lawrence Berkeley National Lab.

6

RESEARCH AND DEVELOPMENT FOR FUTURE LXE TPCS

6.1 TEST BED DESCRIPTION

This section describes

6.1.1 EXPERIMENTAL VESSEL

6.1.2 SLOW CONTROL

6.1.3 DATA ACQUISITION

6.1.4 CHARGE AMPLIFIERS

6.2 HIGH VOLTAGE FEEDTHROUGH DESIGN

A significant amount of time was spent developing and testing High Voltage (HV) feedthroughs for the test bed. This section describes a few of the feedthroughs that were unsuccessful, leading to the final design, which is capable of delivering -11kV to the cathode with no observable breakdown or other effects. Extensive detail of the tests and procedures are not provided. Instead, the following vignettes are intended as an overview to be useful to a student tasked with designing a HV feedthrough.

6.2.1 IMPLEMENTING SHV FEED THROUGHS FROM VACUUM SUPPLIERS

The first attempts at building feedthroughs were to use off-the-shelf products from typical vacuum supply vendors such as MDC and Kurt Lesker. Vacuum HV feedthroughs are intended to for use from air to vacuum, not air to Liquid Xenon (LXe), so it is not surprising that these were not successful. Additionally, by combining ceramic and metal (typically aluminum, stainless steel, nickel, copper) they are especially prone to breakdown at the meeting of these different materials, known colloquially as "triple points". When there are interfaces between materials with different permittivities (dielectric constants), the electric fields are distorted. Field is pushed out of the higher dielectric material into the lower dielectric material. This creates a field enhancement where peak fields can be much higher than average fields in the system. The field enhancement from "triple points" where there is in interface between a conductor and two dielectrics (e.g a plastic or ceramic feedthrough insulator and a gas or liquid) is a common source of breakdown along insulator surfaces. Good design practices, namely choices of geometry reduce the field enhancements in these regions.

Note that ceramic feedthroughs are not appropriate for low background experiments due to high radioactivity , but for test bed work they may be used.

The first few feed throughs used a 12kV Safe High Voltage (a manufacturing identification) (SHV) weldable feed though as shown in Figure 1. If used as operation is intended, the side indicated by A is used on the vacuum-side and B connects to the voltage supply. Instead, we trimmed the long B side and attached a copper, screw-port connector to make the 90 degree connection from vertical feed through to horizontal grid. This was done to avoid placing a conducting surface at high voltage (the tip of side A) in gaseous xenon, thereby increasing the risk of breakdown to the walls of the detector. The feed through's vertical placement is designed such that the copper connector is fully submersed in LXe.

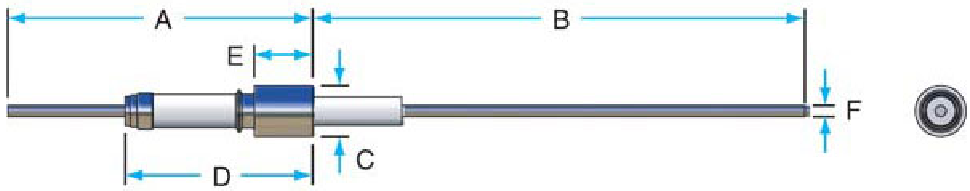

Figure 1: A 12kV SHV weldable connector from vacuum supplier Kurt Lesker.

Feed throughs were tested by performing a cool down, ramping the HV supply slowly, and watching an oscilloscope for a higher than baseline photon rate Figure 6 or a full xenon breakdown Figure 7. We also tested the effect of raising the voltage on the HV supply at a specific rate, and determined that the extremely slow and steady rate of a computer program was not necessarily superior to the imperfect method of the human experimenter – the construction of the feed through, itself, outweighed gains from computer supervised voltage ramping.

Figure 2: 12kV SHV weldable connector, inverted, clipped, and attached with a machined copper connector. The connector uses a screw to capture the SHV feed though, and the same screw to capture a stranded wire, visible in this picture, which is then fed through a hole drilled in the PTFE to connect to the wire grid frames. The wire was wrapped around the grid frame.

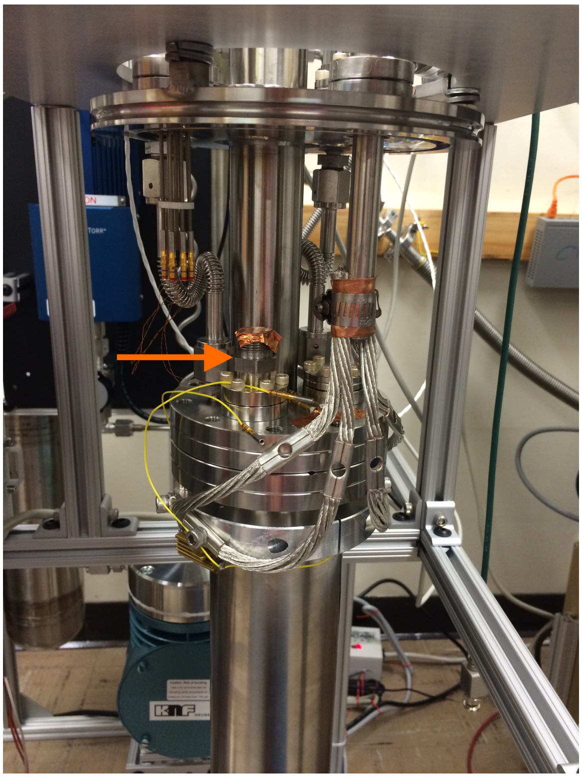

Figure 3: The copper tape in this picture is sitting on top of a 1/2 -in swage connector. The swage connector captures a 1/2 in pipe, which has the 12kV SHV feedthrough welded to the end.

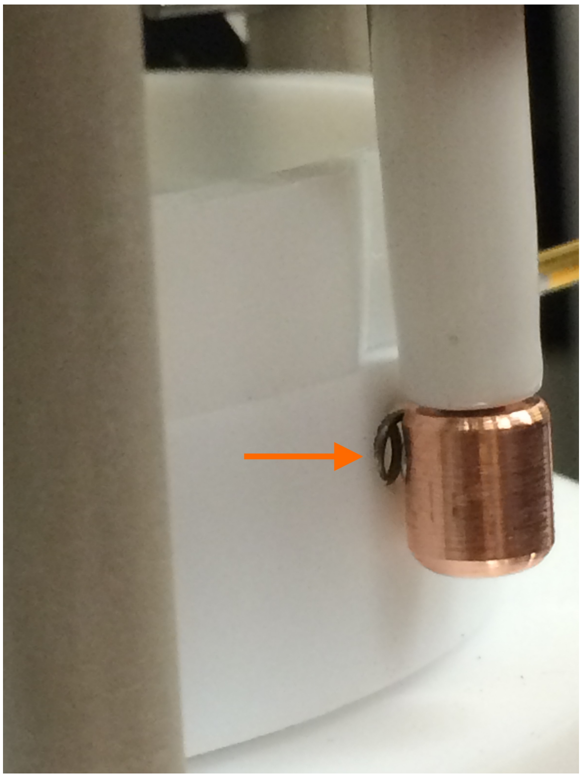

Figure 4: The same 12kV SHV feed through, now with a modified spring connection connecting the feed through to the grid frame.

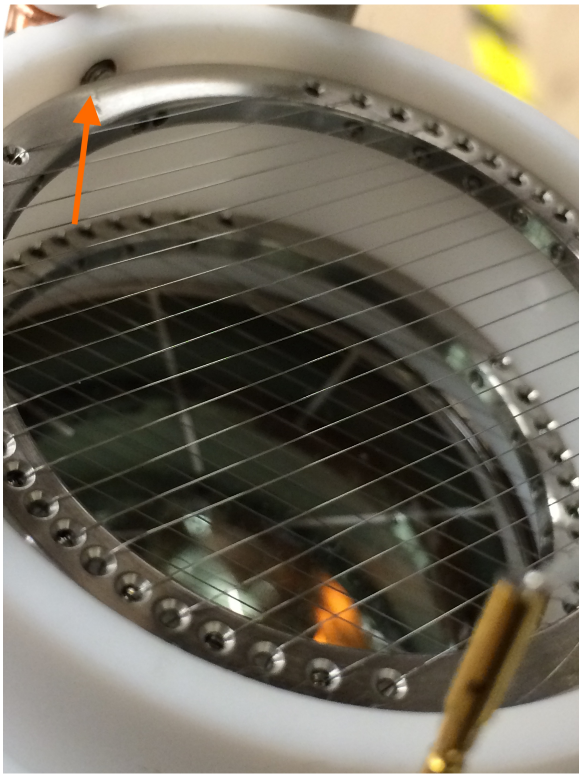

Figure 5: A close up of the cathode grid, showing the spring connection.

Figure 6: Oscilloscope showing baseline rate of single photons (left) compared to a high rate of single photons (right) caused by the high voltage feed through.

Figure 7: Full xenon breakdown as visible on the PMT trace. The large, saturated pulse is caused by the high intensity of light. This type of breakdown was often accompanied by an audible buzz, and a rise in current that would initiate a trip of the high voltage supply.

Iterations of the 12kV SHV feed though were not able to reach more than about 9kV, and not more than about 7kV for extended periods of time like those that would be required for data acquisition. A summary of the issues with this type of feed through design is given below:

- Gas gaps
- Triple points
- Prone to aging

We also tried a stock 20kV SHV feed through with a custom end cap designed by a HV engineer, meant to smooth out typical triple point issues. This feed through was mounted on a CF flange far from the active region. A length of cable was stripped of grounding sheath for its entire length. A small section on one end was stripped of dielectric, this end was tied to the SHV feed though with copper wire, and the custom end cap was placed over this. The side of the cable making the connection to the cathode grid was drilled out for a short length on the bottom, leaving only a tube of dielectric with no conductor. A threaded rod was inserted into the cable, such that the rod made contact with the conductor. The cathode grid frame was screwed onto the threaded rod. The SHV-20 feed though is summarized in pictures in Figure 8, and was found to hold sufficient voltage (10kV) for extended periods of time. However, it was found that the voltage capability of this feed though decreased over time; this is discussed in the next section.

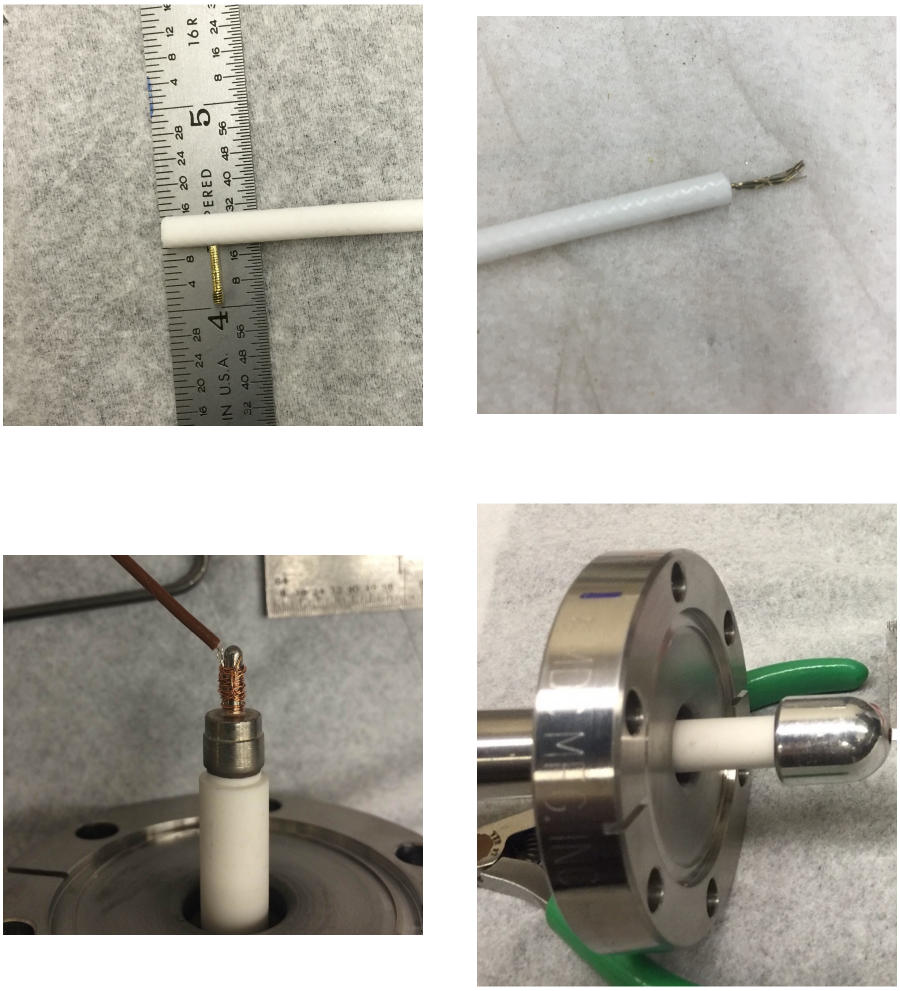

Figure 8: Top: (left) cathode connection side (right) SHV-20 connection side Bottom: (left) an example showing how the cable was attached to the stock SHV-20 feed though end (right) a custom cap fit over the connection, smoothing out triple points.

6.2.1.1 FEEDTHROUGH AGING

It was noticed during subsequent operation that the SHV-20 feed through was subject to some sort of aging process (black line in Figure 10). A month of use resulted in noticeably lower voltage capabilities. The issue could have been any point along the entire voltage chain: feed through - custom cap - connection to cable - cable - connection to grid - grid. Tests focusing on different parts of the voltage chain didn't reveal any weak points. Instead, it was found that the SHV-20 feed though, itself, was subject to aging (red line in Figure 10).

Figure 9: Effect of holing the feed through in place with PEEK zip ties was explored, effects were minimal.

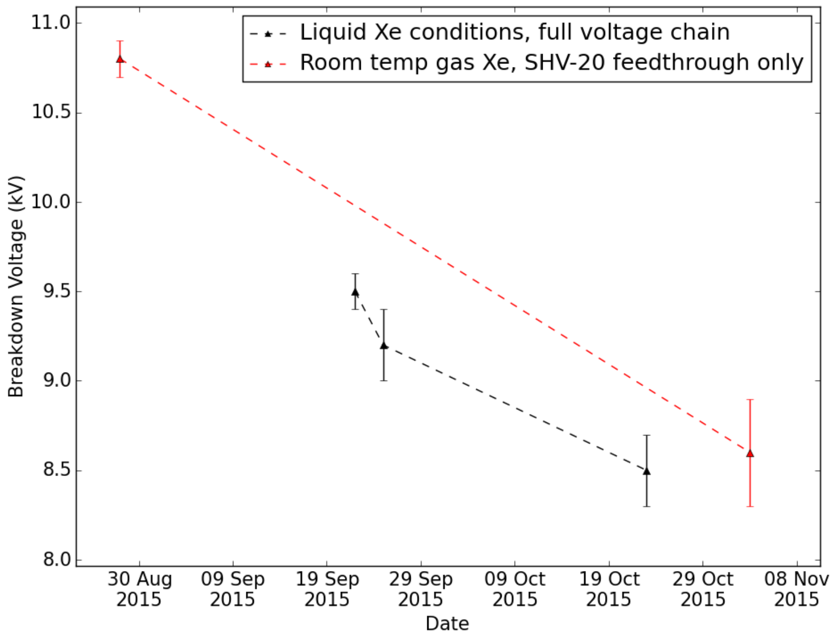

Figure 10: The black line shows the aging observed in the course of normal operations. The red line shows breakdown tests of the SHV-20 feed though in gas, illustrating that the aging observed during operation was due to aging of the feed though.

Feedthrough aging can be the result of arcing and discharges which cause local heating and carbonization of an insulator surface. Once there is a carbon path, the insulator is considered ”tracked” and then holds a much lower voltage than before. Sophisticated HV systems keep peak currents and fault energies to a minimum using series resistors. In this way, a breakdown event does not degrade system performance in the future. In addition to carbon tracks, there can also be insulator degradation from exposure to UV if there is ionization in the region. Xenon ionization is in the UV region of the spectrum, and so any ionization near a feed though insulator may degrade the feed through performance. In the case of this particular feed though, the high field which caused the breakdowns or ionization was likely a result of poor triple-point geometry.

6.2.2 CUSTOM FEEDTHROUGHS

7

SOLUBILITY OF RADON DAUGHTERS IN LIQUID XENON

Rare-event searches are very sensitive to backgrounds from radioactivity in and on detector materials. Some of the most omnipresent and troublesome are ^{222}Rn and its daughters. Decay products from ^{222}Rn plate out on detector surfaces and have typically been assumed to be imbedded and fixed there. We report evidence that radon daughters can dissolve in liquid xenon.

7.1 MOTIVATION

Radon and radon daughters produce problematic backgrounds for rare-event searches [1]. Of particular concern for liquid xenon dark matter detectors are "naked" beta decays. These ground-state to ground-state decays have no accompanying gammas and cannot be rejected via coincidence tagging. Rejection of these backgrounds in WIMP search experiments relies solely on being able to discriminate electron recoils from nuclear recoils. The ^{222}Rn chain contains ^{210}Pb ($T_{1/2}$ = 22.23 y), effectively splitting the decay chain into a "fast chain" and "slow chain" (Fig. 11). Radon can be introduced via two pathways: (1) during detector operation and (2) during detector construction (see Fig. 12). Great care is taken to ensure minimal contamination via pathway 1 because the fast chain naked betas, ^{214}Pb and ^{214}Bi (10%), may decay in the fiducial volume before the purification system can remove them or before they can plate out on detector surfaces. In pathway 2, ^{222}Rn and daughters plate out and onto detector surfaces. Models for plate out can be found in [2] and [3]. The term plate out indicates a chemical bond of some strength, as opposed to daughters 'sitting' on a surface that can be easily washed off. Typically it is assumed that once ^{222}Rn and daughters plate out, they remain stuck to the surface or imbedded in detector materials, and can be rejected by a fiducial volume cut. This means that the slow chain naked betas of ^{210}Pb and ^{210}Bi are assumed to occur outside the fiducial volume. However, evidence of ^{210}Bi mobility has been observed in the liquid scintillator environment of KamLAND [4], [5] and Borexino [6]. If radon daughters are soluble in liquid xenon, the late chain naked betas pose a serious background distributed throughout the fiducial volume.

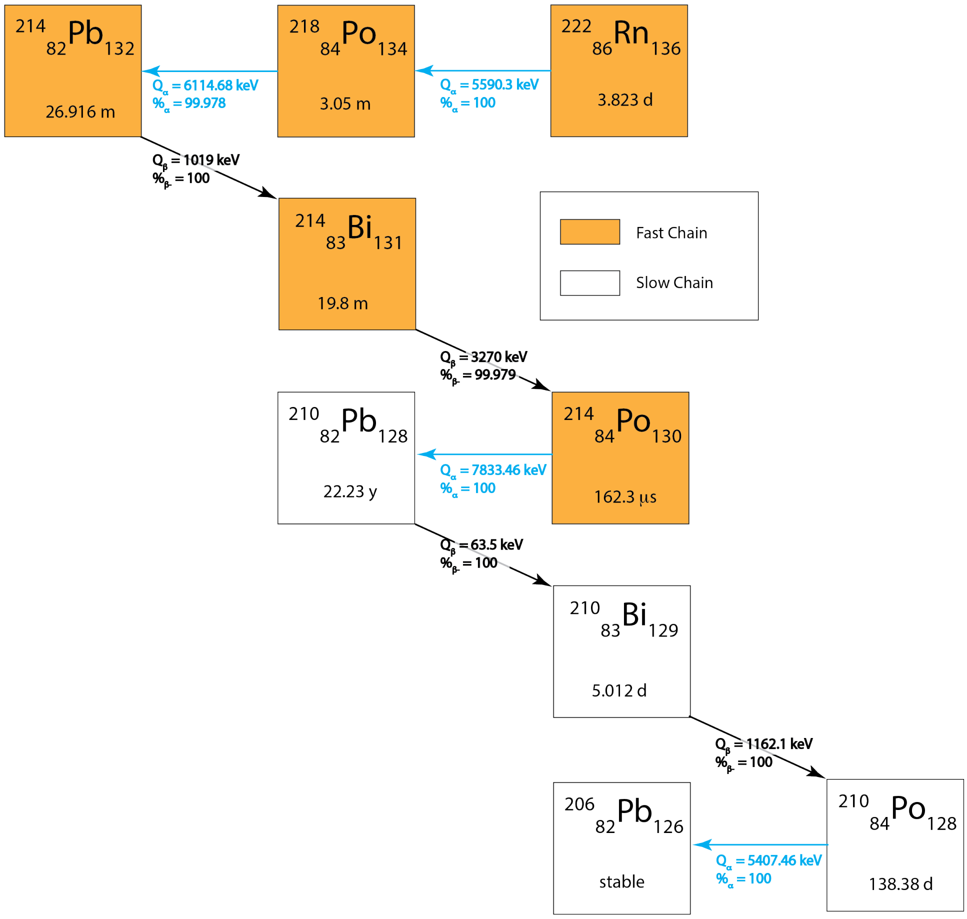

Figure 11: The ^{222}Rn decay scheme. The fast and slow chains are indicated.

In order to investigate the solubility of radon daughters in liquid xenon, a ^{220}Rn source was employed. The analogous long lived daughter in this chain, ^{212}Pb, has a half-life of 10.6 h, making it appropriate for a laboratory test. Investigating pathway 1 in the laboratory will necessarily yield inconclusive results, because it is impossible to tell if the daughter decay of interest plated out before decaying. Therefore, pathway 2 is the focus of this study.

Xenon gas was circulated through the ^{220}Rn source and detector components for a period of >24 h. The detector was then evacuated, thereby assuring the initial position of radon daughters on a detector surface. Any radon daughters subsequently observed in the bulk region after condensing liquid xenon must therefore have dissolved.

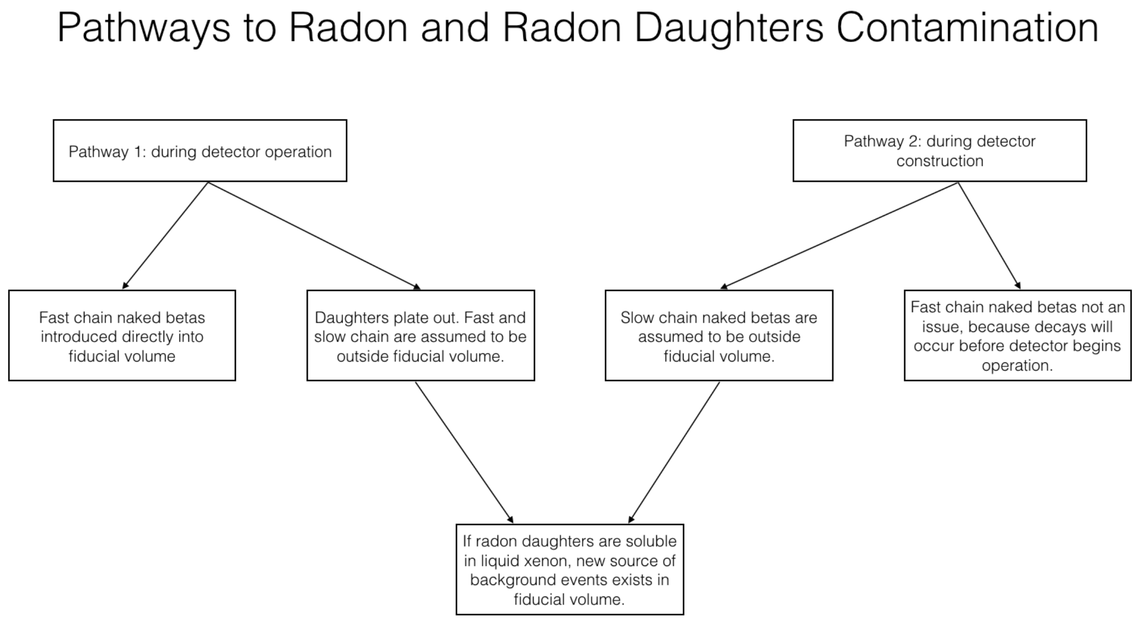

Figure 12: Pathways to radon and radon daughter contamination.

7.1.1 PLATE OUT

Other people have observed different types of ”plate out”. Add citations and summaries here.

7.2 EXPERIMENTAL CONFIGURATION AND METHOD

A diagram of the TPC for this work is shown in Fig. 13. A 50 mm diameter cathode wire grid, extraction wire grid, and a planar, segmented anode were held in Teflon PTFE housing. The anode was instrumented with charge-sensitive preamplifiers. Both grids were constructed from a stainless steel frame strung with 4 μm diameter stainless steel wire on a 2 mm pitch. The xenon inlet was a PTFE tube which introduces xenon gas into the liquid region where it is condensed. The xenon liquid outlet was a thin stainless steel capillary that draws liquid from the TPC into the purification system. Both inlet and outlet tubes were placed near holes drilled in the PTFE to aid circulation into the active volume.

A particle interaction in the liquid xenon volume produced primary scintillation photons (S1) and ionization electrons. The ionization electrons were drifted with an electric field into the gas phase, where they produced secondary scintillation light (S2). A single Hamamatsu R8778 VUV-sensitive PMT was installed in Teflon PTFE housing, facing upward

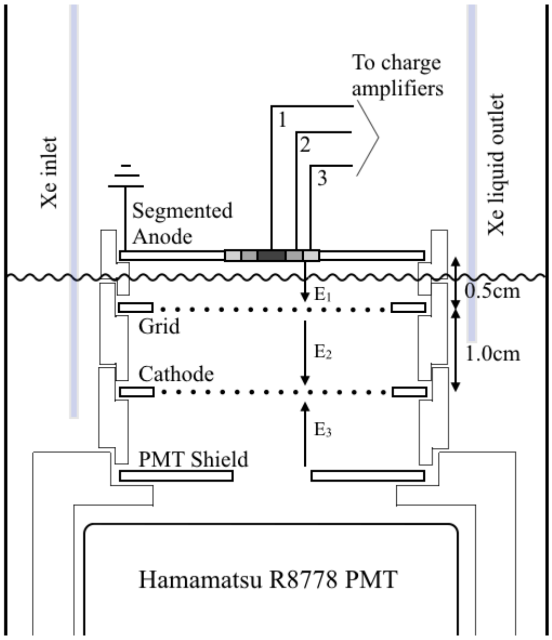

Figure 13: Diagram of the test bed. For this study, the cathode is held at -6.0 kV, and the grid is held at -4.0 kV. E_1^{liq} ≈5.0 kV/cm, E_1^{gas} ≈10.0 kV/cm E_2 = 1.0 kV/cm. E_3 = 2.7 kV/cm. The large gray regions represent the structural rings of PTFE. The line between the grid and anode represents the liquid xenon level. The xenon inlet pipes incoming gas directly into the liquid region, and the liquid outlet pulls from the level of the active region. A gas outlet (not pictured) also draws xenon gas into the circulation system to be purified.

to view the active region. Directly above the PMT was a copper shield mask, held at the same voltage as the PMT bias of -1250 V.

The TPC was filled with 1.5 bar of xenon gas at room temperature. The gas was circulated continuously through the TPC and a heated zirconium getter for at least 24 hours to remove contaminants. The TPC was then cooled to $-100°$ C while circulating xenon gas. Circulation was stopped, and xenon was condensed into the TPC until the liquid level rose to between the extraction grid and anode. The process of filling the TPC took 4 to 5 hours. The liquid level was kept stable by keeping the temperature and pressure constant in the TPC. During data collection, xenon from the TPC was circulated through a getter and re-condensed into the TPC to remove impurities.

7.2.1 PLATE OUT OF ^{220}RN DAUGHTERS

The procedure to plate out ^{220}Rn daughters on the inner surfaces of the detector was the same as described in Sec. **??**, except that the circulation path was directed through a 2 kBq ^{220}Rn source. The ^{220}Rn is shown

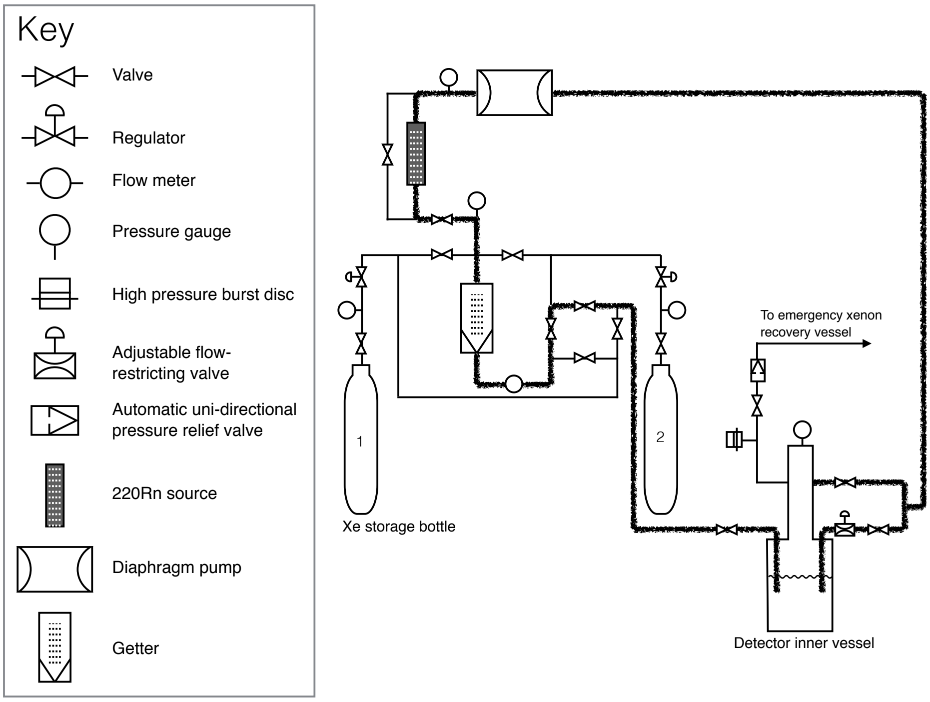

Figure 14: An example a circulation path used for plate out is shown on the pumping and instrumentation diagram. During data-taking the radon source was bypassed. The typical liquid level is indicated on the diagram to show that the outlet drew from the liquid via a capillary, ensuring purification of the liquid xenon. A gas purge also purified the gas column in the detector.

in Fig. 15. The rate of radon activity in the TPC was measured to be 4.5 ± 0.5 Hz during plate out. The total alpha rate was measured by taking repeated 1200 ms traces on an oscilloscope of the PMT with a falling edge trigger and counting the alpha decays. This rate was then halved to get the rate of radon decays. The 4.5 ± 0.5 Hz rate of radon activity represents activity for all of the space internal to the PTFE support structure. Decay daughters diffused until they contacted a wall or other surface, where they could plate out. Some percentage of decay daughters are expected to be positively charged ions. If the cathode grid was biased, charged decay daughters drifted preferentially to the cathode grid. The cathode voltage during plate outs is noted in Table 1.

Prior to filling the TPC with liquid xenon, the circulation was stopped and the xenon gas removed from the TPC and the circulation lines. A vacuum pressure of a few 10^{-4} Torr was achieved in a period of ten minutes. This step ensured removal of ^{220}Rn and decay daughters which are dissolved in the gas, leaving only those daughters which had plated out on a detector surface. Since the fill time of the TPC is 4 to 5 hours, there

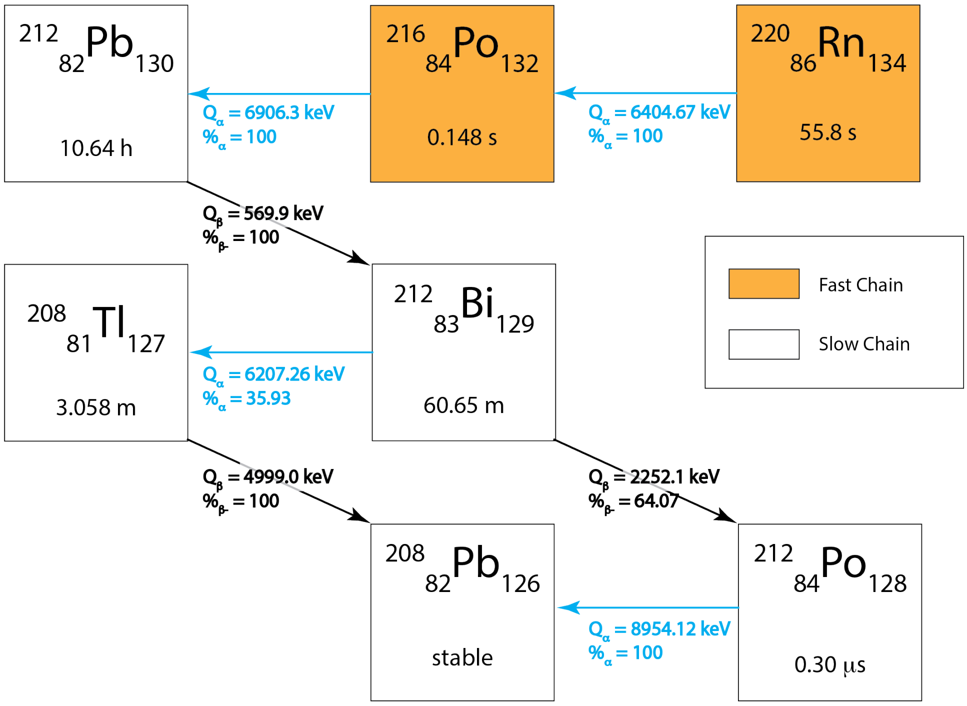

Figure 15: The ^{220}Rn decay scheme. The fast and slow chains are indicated. Events in the plate out data sets are from the slow chain.

were no fast chain alpha decays of ^{220}Rn and ^{216}Po in the plate out data. Additional details are summarized in Table 1.

7.2.2 DATA COLLECTION

Voltage records from PMT and charge channels were collected with a 14-bit ADC with 125 MHz sampling and a 20 MHz low-pass filter. The trigger was a coincidence between the PMT and the central anode segment, used to select events in the central ($r < 6$ mm) column of xenon. This avoids any electric field fringing effects.

7.2.3 CALIBRATION

In order to identify a signal region for bulk radon daughters, the flow though ^{220}Rn source was employed directly following dataset A, allowing ^{220}Rn to flow into the liquid bulk of the TPC. The bulk daughter decay of interest, ^{212}Bi alpha, has an energy approximately equal to the ^{220}Rn alpha decay. The alpha signals were sufficient to saturate the biasing circuit of the PMT, so alpha decays within 1 MeV of each other were indistinguishable. Therefore, the region in S1 area vs. S2 area where the ^{220}Rn alphas appeared was also where ^{212}Bi alphas were expected (Fig. **??**).

	dataset ID	A	B	C	D
Plate-Out Conditions	Circulation through ^{220}Rn Source	yes	yes	no	-
	Circulation Time (h)	24	48	24	-
	Cathode Voltage (kV)	-1	0	0	-
Data-Taking Conditions	Circulation through ^{220}Rn Source	no	no	no	yes
	Cathode Voltage (kV)	-6	-6	-6	-6
	Grid Voltage (kV)	-4	-4	-4	-4
	Approximate Live Time (h)	13	25	25	1

Table 1: Summary of plate out and data-taking conditions. Data sets A and B are taken after circulating radon gas and data set C, background, had no radon circulation. Data set D was taken following dataset A, and radon was circulated in a liquid xenon environment, purposefully introducing radon into the detector bulk to calibrate the detector.

7.2.4 POSITION RECONSTRUCTION

The central anode segment was assumed to select events from the central column with 100% efficiency. Events occurring under one of the outer concentric segments can produce a signal on the central anode. This uncertainty is taken into account in the calculation of fiducial volume. The drift time of the events was calculated from the difference between the S1 and S2 pulses.

7.3 ANALYSIS

7.3.1 NUMBER OF ^{220}RN DAUGHTERS IN THE TPC

As described in Sec. 7.2.1, the rate of ^{220}Rn in the TPC was measured to be 4.5 ± 0.5 Hz during plate out. From this, the number of daughter atoms ^{212}Pb and ^{212}Bi present in the TPC just prior to filling the liquid xenon were calculated. The number of daughter atoms as a function of the plate out time is shown in Fig. 16 along with the data acquisition periods for each dataset. This calculation assumes that the diffusion time in the PTFE walls was less than removal time via the capillary.

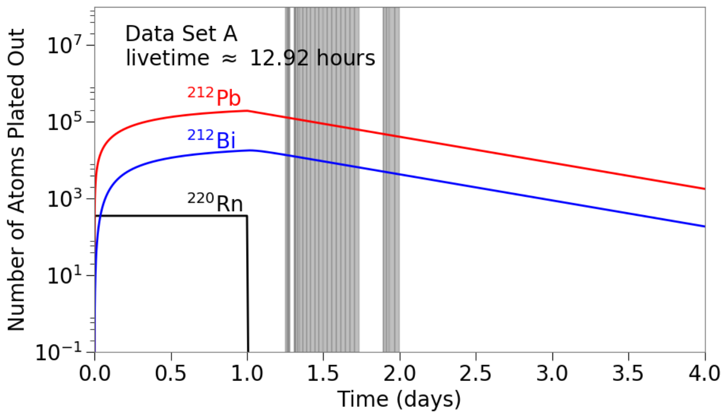

(a)

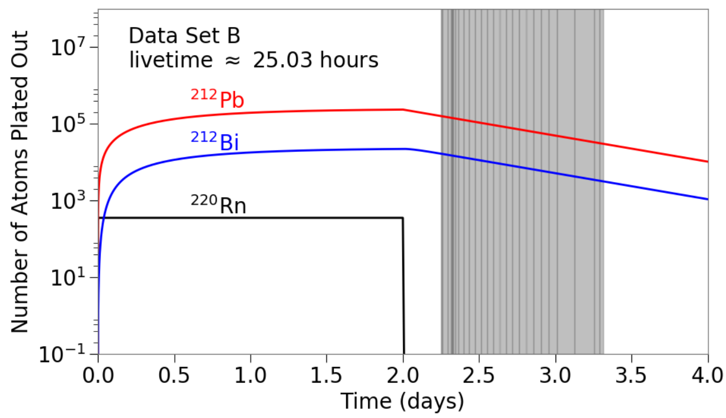

(b)

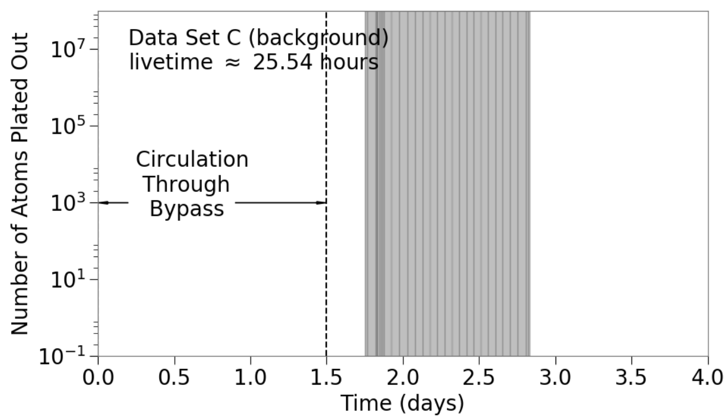

(c)

Figure 16: a) and (b) and (c) show the plateout conditions of datasets A, B, and C, respectively. The gray bands indicate time when data was being acquired. Dataset D (calibration) was taken following dataset A and consisted of a few hours.

7.3.2 DATA SELECTION

The trigger described in Sec. 7.2.2 captured the slow chain decays as shown in Fig. 15. The ^{212}Bi beta decay is followed by the 300 ns alpha decay of ^{212}Po; these decays are referred to herein as "Bi-Po".

The aim of this analysis was to reconstruct the z-position of radon daughter alpha decays via the timing difference between the S1 and S2 of an event. Therefore, Bi-Po events were rejected, as the two S2s presented a timing ambiguity. The focus was instead on identifying ^{212}Bi alpha decays. All events were expected to take place on detector surfaces, so ^{212}Bi alpha decays in the drift region indicate mobility of plated-out daughters ^{212}Pb and/or ^{212}Bi; it was not possible to determine whether the original position was on the cathode wires, PTFE walls, or other detector surface.

The software cuts used to select ^{212}Bi alphas are described below:

1. **Data Cleaning** Remove events with any railed charge channel.

2. **Fiducialization** Require more signal in the central anode segment than the other two concentric anode segments.

3. **Select Alpha Events** The tallest pulse in an event was required to be an S1. Alphas are higher energy than the other decays in the ^{220}Rn chain, and have a characteristically high light yield, so this cut is generous in keeping all alpha events.

4. **Reject Bi-Po Topology** Of the alpha events, those with one S1 and one S2 (single-scatter) were classified as ^{212}Bi alpha. Events with two S1s (one of which is alpha-like), and one or two S2s were classified as Bi-Po.

5. **Reject Bi-Po Energy** There are two ways a Bi-Po event can mimic the topology of ^{212}Bi alpha: (i) alpha decay was prompt and so the scintillation signals from the beta and alpha were combined into one large S1 (ii) the beta was ejected into the cathode wire and therefore there was no signal detectable from the beta. To robustly identify ^{212}Bi, the alpha S1 areas of ^{212}Bi alpha and Bi-Po events from Step 2 were histogrammed and fit with Gaussian functions. ^{212}Bi alpha events were tightly selected with a high and low S1 area cut placed on single-scatter alpha events: anything above $(\mu - 3\sigma)_{Bi-Po}$ was considered a Bi-Po event and anything below $(\mu - 3\sigma)_{Bi-alpha}$ was considered a beta or gamma, and discarded (Fig. 17).

6. **Z-position Cut** Events in the cathode region were separated from events in the bulk region with a z-position cut (discussed further below).

7. **Bulk Signal Area Cut** Only ^{212}Bi alpha tagged events which also fell in a signal region expected from calibration with the ^{220}Rn flow though source (Fig. **??**) were considered to be daughters which have dissolved.

In order to choose the value for the z-position cut in Step 4, a Monte Carlo approach was used. A Bi-Po decay with a prompt alpha (appears as single-scatter) where the beta penetrates into the bulk region, could mimic a ^{212}Bi alpha bulk event. To better understand Bi-Po cathode events and the danger of mis-identifying them as ^{212}Bi alphas in bulk, a Monte Carlo study was done with the ^{212}Bi beta spectrum (the highest energy beta in the ^{220}Rn chain) to determine the maximum distance a beta could penetrate into the bulk region. The study yielded a maximum beta penetration of $zmax_{MC} = 0.12$ cm, see Fig. 18. The z position cut separating cathode from bulk was then defined to be $z_{cut} = zmax_{MC} + 3\sigma_{fit}$, where σ_{fit} is just the width of a Gaussian fit for the position of the cathode. Figures **??** and **??** show the cathode position fits as well the the location of z_{cut}. The cathode position fit error, σ_{fit}, was the same for both datasets A and B, and was also used to determine z_{cut} for the background and calibration sets.

One feature that merits further discussion from 19 is the strong anti-correlation in S1 Pulse Area vs. S2 Pulse Area apparent in cathode events. The cathode region was subject to very high, non-uniform fields due to the thin wires that comprised the cathode grid. Events that occurred on the wires encountered different fields depending on their position on the surface of the wire. Additionally, two events that occurred at exactly the same spot encountered different fields depending on which direction the decay particle (alpha, beta, etc.) traveled. The amount of scintillation and ionization from an interaction in liquid xenon depends on the field at the interaction site. Higher fields result in more ionization electrons being separated from the interaction site and therefore more S2. Mono-energetic events occurring in a uniform field have small anti-correlated fluctuations in S1 and S2 size. Non-uniform fields greatly exaggerate the typical variation in S1 and S2 size resulting in the spread out cathode region (blue) observed in Figures **??**, **??**, and **??**. Events in the bulk region encounter a relatively low, uniform field resulting in a compact signal region in S1 vs. S2 (red region in **??**.

7.4 RESULTS AND DISCUSSION

We observed 11 bulk ^{212}Bi alphas for dataset A, 20 for dataset B, and 1 background event in the signal region from dataset C. The counts of cathode region ^{212}Bi alphas are presented in Table 2. There was only one back-

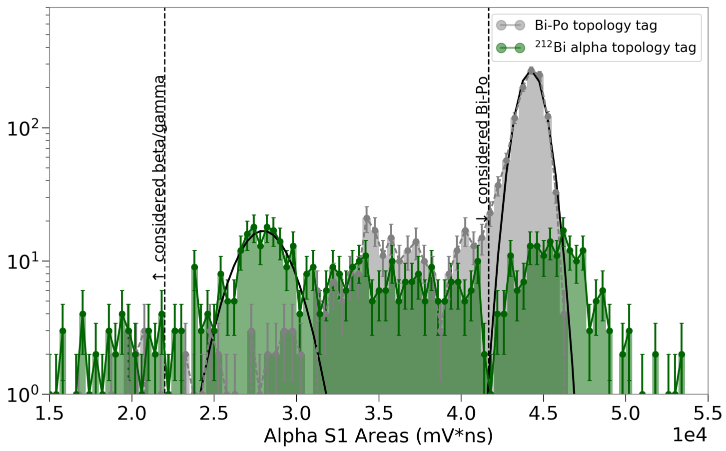

(a)

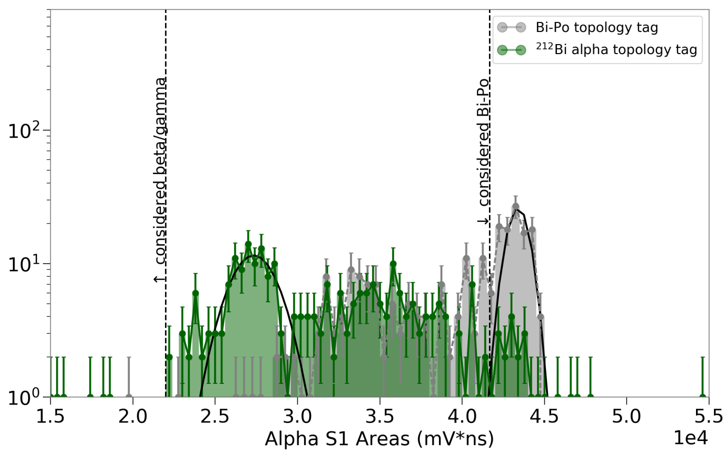

(b)

Figure 17: The S1 areas of events that were tagged using topological features. These distributions were then used to employ the cuts in Step 3. The branching ratio for ^{212}Bi is 36:64 for α:Bi-Po. Dataset (a) showed 10:90 and dataset (b) showed 35:65. It is unclear why the branching ratios for dataset (a) deviate so much from expectation. The trigger is more efficient for Bi-Po events because those decays would produce more a larger charge signal. It's possible that the cathode being left on during the plate out procedure had some effect on the geometrical distribution of daughters on the cathode wires, which further biased the trigger.

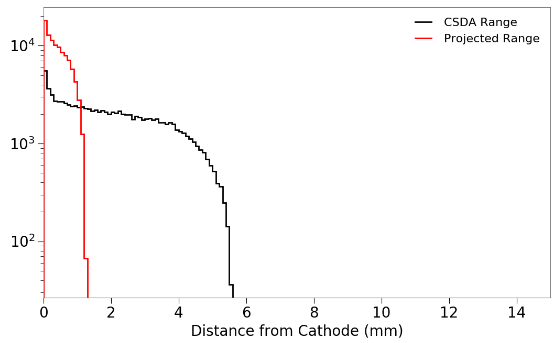

Figure 18: Monte Carlo study to find the maximum distance a ^{212}Bi beta (2.2 MeV) on the cathode could penetrate into the drift region. The projected range (red) is the relevant curve for this analysis; it shows a beta is not expected to travel more than 1.2mm from the cathode.

ground event observed in the signal region, so with 95% confidence the true background count is at most 4.74. The observed counts for dataset A and B lie far above the 95% confidence limit for background, indicating they are true observations of ^{212}Bi alphas in bulk. The dissolved fraction of ^{212}Bi alphas for dataset A (≈ 13 h livetime) is 0.035 ± 0.010, and for data set B (≈ 25 h livetime) is 0.099 ± 0.020.

These results indicate that either ^{212}Pb or ^{212}Bi itself is soluble to a small degree in liquid xenon.

Table 2: Number of detected alpha particle events whose energy determination was consistent with ^{212}Bi decay to ^{208}Tl. Live times are quoted in Table 1

dataset ID:	A	B	C
Bulk Events	11	20	1
Cathode Events	300	183	4

The solubility calculation is subject to errors from the following things:
- Number of Measuring it gives:

0.1μ Bq/kg LXe for ^{212}Bi mobility in LUX (not published, but this number is in the LZ projected sensitivity paper)

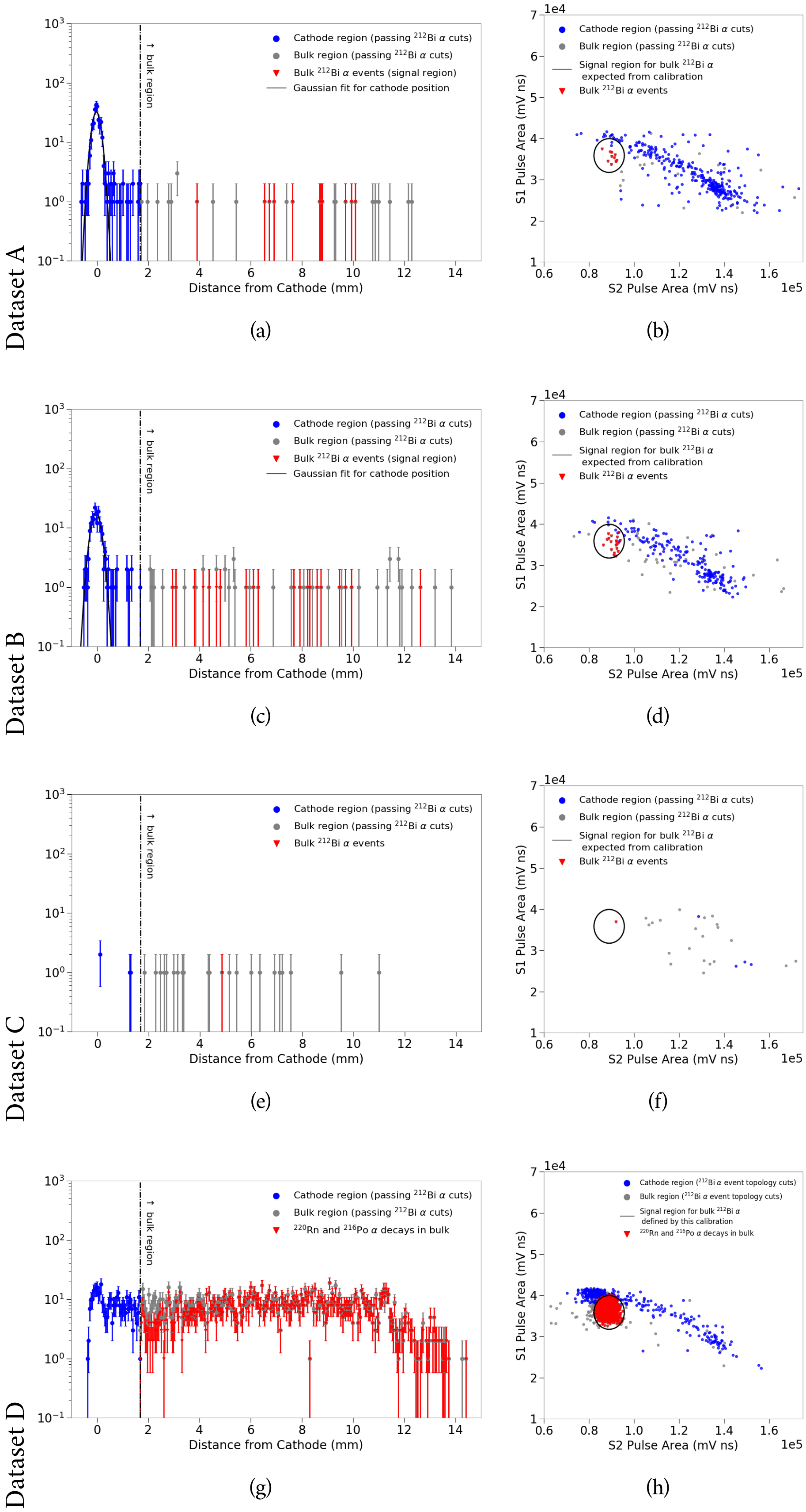

Figure 19: **(left)** Distribution of events in z. **(right)** The same events distributed in the S1-S2 plane, showing selection criteria for candidate ^{212}Bi alpha events in the bulk liquid xenon.

Table 3: Solubility of ^{212}Bi in liquid xenon.

dataset ID:	A	B
Plated Out	??Bq/cm^2	??Bq/cm^2
Dissolved	??Bq/kg	??Bq/kg
Dissolved Fraction		

7.5 CONCLUSION

This article has presented the first evidence that the ^{220}Rn daughters ^{212}Pb and/or ^{212}Bi are soluble in liquid xenon. The dissolved events are a small fraction of events that are plated-out on detector surfaces. These daughters are proxies for the isotopes ^{210}Pb and/or ^{210}Bi, which undergo naked beta decays in the ^{222}Rn chain and pose a problem for liquid xenon dark matter detectors. Our study counts dissolved ^{212}Bi alpha events as well as ^{212}Bi alphas plated out on the cathode. We observed a dissolved fraction of 0.035 ± 0.010 for dataset A, and 0.099 ± 0.020 for dataset B (a summary of data taking and plate-out conditions is in Table 1). Further study, where a known amount of ^{220}Rn daughters are plated out on a known area is necessary to measure dissolution rates. Additional studies that compare the solubility of radon daughters adsorbed on different materials would also be useful.

During detector construction, ^{222}Rn and daughters plate out onto detector surfaces. During operation, ^{222}Rn enters the detector via the circulation system. These daughters can also plate out onto detector surfaces to dissolve into the fiducial volume at a later date, where they can decay. Our study focuses on the former mode, because laboratory results of the latter would be inconclusive. However, we expect radon daughters to be soluble regardless of the plate out occurring in a gas or liquid environment.

8

ELECTRON TRAIN STUDIES

8.1 ELECTRON TRAIN STUDIES

8.1.1 MOTIVATION

8.1.2 EXPERIMENTAL CONFIGURATION

8.1.3 RESULTS

PART IV

APPENDIX

A

DUMMY APPENDIX

BIBLIOGRAPHY

[1] D.S. Akerib et al. "Radiogenic and muon-induced backgrounds in the LUX dark matter detector". In: *Astropart. Phys.* **62**: (2015), pp. 33–46. ISSN: 09276505. arXiv: 1403.1299. URL: http://dx.doi.org/10.1016/j.astropartphys.2014.07.009http://linkinghub.elsevier.com/retrieve/pii/S0927650514001054.

[2] V. E. Guiseppe, S. R. Elliott, A. Hime, K. Rielage, and S. Westerdale. "A Radon Progeny Deposition Model". In: 2011, pp. 95–100. URL: http://aip.scitation.org/doi/abs/10.1063/1.3579565.

[3] E. O. Knutson. "Radon and Its Decay Products in Indoor Air". Wiley, 1988.

[4] Yasuhiro Takemoto. "7Be solar neutrino observation with KamLAND". In: *Nucl. Part. Phys. Proc.* **265-266**: (2015), pp. 139–142. ISSN: 24056014. URL: http://linkinghub.elsevier.com/retrieve/pii/S2405601415003788.

[5] A. Gando et al. "<math> <mmultiscripts> <mi mathvariant="normal">Be</mi> <mprescripts/> <none/> <mn>7</mn> </mmultiscripts> </math> solar neutrino measurement with KamLAND". In: *Phys. Rev. C* **92**:5 (2015), p. 055808. ISSN: 0556-2813. URL: https://link.aps.org/doi/10.1103/PhysRevC.92.055808.

[6] G. Bellini et al. "Final results of Borexino Phase-I on low-energy solar neutrino spectroscopy". In: *Phys. Rev. D* **89**:11 (2014), p. 112007. ISSN: 1550-7998. URL: https://link.aps.org/doi/10.1103/PhysRevD.89.112007.